Neurobiology of Disease 226 (2026) 107473

Contents lists available at ScienceDirect

Neurobiology of Disease

journal homepage: www.elsevier.com/locate/ynbdi

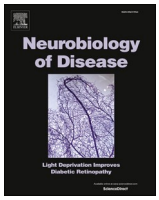

PBMC DEG/miRNA biomarkers of TDP-43 pathology in ALS

Maria Francesca Manchinu [a], Michela Congiu [b,a], Matteo Massidda [a], Giuseppe Borghero [c,d,i], Jacopo Marongiu [b], Isabella Marzi [e], Andrea Maschio [a], Vincenzo Rallo [a], Marcello Serra [b], Clara Porcedda [b], Michela Etzi [b], Maria Francesca Palmas [b], Andrea Angius [a], Valeria Sogos [b,d], Maria Ida Pateri [c,i], Maristella Steri [a], Valentina Coroneo [f], Alfonso De Simone [g], Giovanni Cossu [h], Fabrizio Chiti [e], Anna Rosa Carta [b,a,d,*]

[a] Institute for Genetic and Biomedical Research, The National Research Council (CNR), Monserrato, Italy
[b] Department of Biomedical Sciences, University of Cagliari, Cagliari, Italy
[c] ALS Interdivisional Center, Cagliari, Italy
[d] Interdepartmental Center for ALS and Motor neuron Diseases, University of Cagliari, Cagliari, Italy
[e] Department of Experimental and Clinical Biomedical Sciences, Section of Biochemistry, University of Florence, Florence, Italy
[f] Department of Medical Sciences and Public Health, University of Cagliari, Cagliari, Italy
[g] Department of Pharmacy, University of Naples Federico II, Naples, Italy
[h] Department of Neuroscience, Neurology and Stroke Unit, ARNAS Brotzu, Cagliari, Italy
[i] Neurology UOC, Azienda Ospedaliero-Universitaria di Cagliari, Cagliari, Italy

ARTICLE INFO

Keywords:
Amyotrophic lateral sclerosis
Diagnostic biomarker
PBMC
Transcriptomic
miRNA
TDP-43

ABSTRACT

Amyotrophic lateral sclerosis (ALS) lacks reliable, disease-specific, and minimally invasive biomarkers, representing a major barrier to early diagnosis and patient stratification. The primary aim of this translational pilot study was to identify a disease-specific, TDP-43-related, gene–microRNA (miRNA) signature in peripheral blood mononuclear cells (PBMCs) of ALS patients with potential diagnostic value. To this end, we first identified differentially expressed disease-specific genes (dsDEGs) using a TDP-43–based rat model of ALS, generated by stereotaxic infusion of full-length (FL) TAR DNA-binding protein 43 (TDP-43) into the motor cortex. Transcriptomic profiling of the motor cortex revealed candidate dsDEGs, which were subsequently validated by RT-qPCR in motor cortex, spinal cord, and PBMCs from the same animals.

To assess translational relevance, expression levels of these dsDEGs were analyzed in PBMCs from early- to mid-stage ALS patients and matched healthy controls, while disease specificity was evaluated using Parkinson's disease (PD) samples. In parallel, conserved miRNAs predicted to target the identified dsDEGs were examined in both rat and human PBMCs.

Five dsDEGs, Mctp1, Penk, Mt2A, Drd1, and Rasgrp2, were consistently dysregulated across central and peripheral tissues in the TDP-43 rat model. RT-qPCR analysis of human PBMCs confirmed significant and selective dysregulation of these genes in ALS, but not in PD, supporting disease specificity. Moreover, exposure of human neuroblastoma cells and healthy PBMCs to TDP-43 recapitulated the ALS-like expression changes. Computational and experimental analyses identified seven conserved miRNAs targeting these dsDEGs, of which four were significantly downregulated in ALS PBMCs, supporting a coordinated regulatory network.

Receiver operating characteristic (ROC) analyses demonstrated strong discriminative performance for both the gene signature (AUC 0.87–1.00) and the associated miRNAs (AUC 0.95–1.00). Together, these findings define a novel PBMC-based gene–miRNA signature that mirrors central ALS pathology and shows high diagnostic accuracy and disease specificity, highlighting its potential as a minimally invasive biomarker for ALS.

* Corresponding author at: University of Cagliari - Dept. of Biomedical Sciences, Cittadella Universitaria di Monserrato, Building A, S.P. 8, 09042, Monserrato, Cagliari, Italy.
E-mail address: annarosa.carta@unica.it (A.R. Carta).

https://doi.org/10.1016/j.nbd.2026.107473
Received 1 April 2026; Received in revised form 5 June 2026; Accepted 5 June 2026
Available online 6 June 2026

1. Introduction

Amyotrophic lateral sclerosis (ALS) is a fatal neurodegenerative disorder affecting upper and lower motor neurons in the cerebral cortex, brainstem, and spinal cord, leading to progressive weakness, muscle atrophy and spasticity, ultimately resulting in complete denervation of voluntary muscles (Mead et al., 2023). Disease onset is typically focal, arising in restricted regions of the central nervous system (CNS) and subsequently spreading throughout the motor network as pathology progresses.

A pathological hallmark of most ALS cases, including nearly all sporadic (sALS) and most familiar (fALS) cases, is the presence of cytoplasmic inclusions containing phosphorylated TAR DNA-binding protein 43 (pTDP-43) in neurons and motor nerve biopsies (Prasad et al., 2019; Riva et al., 2022). TDP-43 is a ubiquitously expressed RNA-binding protein involved in multiple aspects of RNA metabolism, including splicing, transport, and stability (Ling, 2018). Among more than 40 genes associated with mutations in ALS, TAR DNA-binding protein gene (TARDBP) mutation is recognized as highly frequent (Renton et al., 2014; Yuan, 2024), with significantly high frequency in specific geographical regions such as Sardinia Island in Italy where, along with the C9orf72 mutation, it is a primary driver of ALS accounting for about 30% of cases (Chiò et al., 2011). TDP-43 pathological mislocalization and aggregation represent a unifying hallmark of ALS, observed in nearly all sALS and most fALS cases. In disease conditions, TDP-43 undergoes nuclear clearance and accumulates in the cytoplasm, where it forms phosphorylated and ubiquitinated aggregates associated with neuronal dysfunction and degeneration (Liu et al., 2017; Klim et al., 2021).

Despite advances in understanding ALS pathophysiology, diagnosis still relies largely on clinical and electrodiagnostic criteria, often resulting in diagnostic delay and uncertainty. The lack of reliable, disease-specific, and minimally invasive molecular biomarkers remains a major limitation, hindering early diagnosis and timely therapeutic intervention (Gwathmey et al., 2023; Richards et al., 2021). Although biofluid markers such as neurofilament light chain reflect axonal degeneration, they lack disease specificity and do not directly capture ALS-related molecular pathological mechanisms (Riva et al., 2022; Sturmey and Malaspina, 2022). The clinical heterogeneity and complex pathological frame of ALS further complicate the identification of disease-specific readouts (Sturmey and Malaspina, 2022).

Peripheral blood mononuclear cells (PBMCs) have emerged as a promising and accessible source of biomarkers, as they recapitulate key aspects of ALS pathology, including TDP-43 mislocalization, altered RNA metabolism, proteostasis-involved proteins, and immune dysregulation (De Marco et al., 2017; Filareti et al., 2017; Luotti et al., 2020; Mosallaei et al., 2022; Nardo et al., 2011; Vega-Benedetti et al., 2024). Consistently, transcriptomic studies have identified numerous differentially expressed genes (DEGs) and microRNAs (miRNAs) in PBMCs from ALS patients, supporting their potential diagnostic and prognostic relevance (Dragoni et al., 2025; Grima et al., 2023; Liguori et al., 2018).

Building on this evidence, the primary aim of this pilot study was to

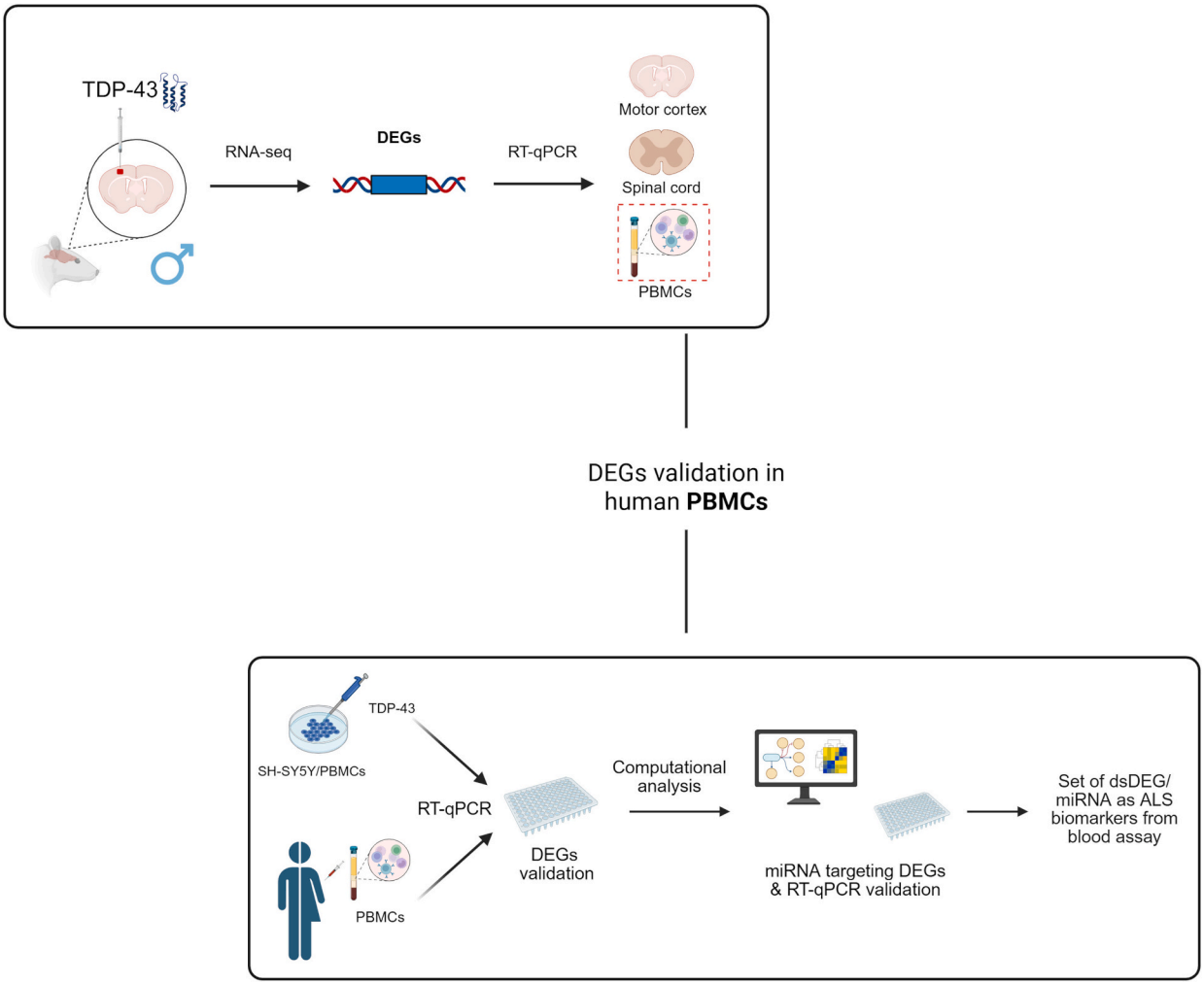

Fig. 1. Experimental workflow.

identify a disease-specific, TDP-43-induced, gene–miRNA signature in PBMCs of ALS patients, with diagnostic value and clear association to ALS neuropathology. To achieve this, we adopted a translational strategy grounded on the central role of TDP-43 proteinopathy. We leveraged a preclinical model in which stereotaxic infusion of exogenous full-length (FL) TDP-43 into the rat primary motor cortex induces ALS-like pathology that propagates from the motor cortex along the motor axis to the spinal cord and peripheral muscles, resulting in motor impairment (Fig. 1). (Marongiu et al., 2026, bioRxiv, 2026.03.27.714692, doi: https://doi.org/10.64898/2026.03.27.714692; Staderini et al., 2022; Vivoli Vega et al., 2019).

Through transcriptomic profiling of the TDP-43–infused rat motor cortex, we first identified a set of TDP-43-associated, putatively disease-specific DEGs (dsDEGs). Following a pathology spread-driven tissue sampling, these candidates were validated by Reverse Transcription Quantitative PCR (RT-qPCR) across central (motor cortex and cervical spinal cord) and peripheral (PBMCs) tissues from the same animals, enabling the selection of dsDEGs consistently reflecting CNS pathology at the peripheral level. Their translational relevance was then assessed in PBMCs from early- to mid-stage ALS patients and matched healthy controls, while disease specificity was evaluated using samples from Parkinson's disease (PD) patients as a distinct neurodegenerative comparator.

To further support the mechanistic link with TDP-43 pathology, the identified gene expression changes were reproduced in human neuroblastoma cells and healthy donor-derived PBMCs exposed to TDP-43. In parallel, given the emerging role of miRNAs in ALS, we identified conserved miRNAs predicted to target the selected dsDEGs and assessed their expression in both rat and human samples (Maity and Kaundal, 2025).

Importantly, the combined dsDEG–miRNA signature in PBMCs demonstrated strong discriminatory power between ALS patients and healthy controls in receiver operating characteristic (ROC) analyses, while also distinguishing ALS from PD, supporting both diagnostic accuracy and disease specificity.

Overall, this pilot study defines a novel PBMC-based gene–miRNA signature that mirrors TDP-43-driven CNS pathology and provides a minimally invasive, disease-specific molecular readout for ALS. These findings represent an important step toward the development of clinically applicable biomarkers for early and accurate ALS diagnosis.

2. Materials and methods

2.1. Animals

Male Sprague–Dawley rats (250–275 g, Envigo) were housed in standard conditions. Procedures were performed in accordance with European Community guidelines (2010/63 UE L 276 20/10/2010) to minimize animal pain, discomfort, and reduce animal number. Rats (TDP-43 $n = 5$, vehicle n = 5) were anesthetized with Fentanyl (3 mg/kg)/medetomidine hydrochloride (0.35 mg/kg) and received a unilateral stereotaxic infusion via a silica microinjector at 1 μL/min with 5 μL of either recombinant purified human FL TDP-43 or vehicle (TDP-43 dissolving buffer: 50 mM HEPES, 0.1% (*w/v*) PEG 3350, 2 mM LDAO, 0.25% OG, 1 M NaCl, pH 8.0), targeted to the primary motor cortex at coordinates relative to bregma: +1.9; 0 mm anteroposterior; ± 2.8; ± 2 mm mediolateral; −1.6 mm beneath the dura). Vehicle-infused animals served as controls.

All animals were sacrificed four months after surgery, with no variation in survival time between individuals. Rats were euthanized by decapitation, and blood pouring from the neck was immediately collected for PBMC isolation. The infused motor cortex and cervical spinal cord were rapidly dissected, immediately immersed in trizol reagent to preserve RNA integrity, and stored at −80 °C until RNA extraction. Cervical spinal cord tissue was collected from the same animals to assess potential propagation of TDP-43–induced molecular alterations along the corticospinal axis, based on preclinical findings showing that FL TDP-43 pathology spreads throughout and beyond the CNS, affecting motor cortex, spinal cord, and peripheral muscles (Marongiu et al., 2026, bioRxiv, 2026.03.27.714692, doi:https://doi.org/10.64898/2026.03.27.714692), in agreement with previous studies (Brettschneider et al., 2013; Porta et al., 2018; Ding et al., 2021).

Extracted RNA from motor cortex samples was subsequently used for transcriptomic analysis and RT-qPCR validation, while cervical spinal cord samples were used for RT-qPCR validation. PBMCs were isolated from whole blood according to established protocols (see dedicated section below) and processed for RNA extraction and gene expression analyses to assess peripheral modulation of dsDEGs.

2.2. Participants

Patients with ALS were all recruited in Sardinia, at a tertiary referral clinic of the Institute of Neurology, University of Cagliari (Table 1, ALS $n = 10$, HC n = 10). The study included ALS patients of Sardinian ancestry (defined as subjects with both parents of Sardinian origin). Study eligibility criteria were diagnosis of ALS and time interval between symptom onset and diagnosis of less than 17 months. Diagnostic criteria: all patients met the revised El Escorial-Arlie House Criteria for ALS diagnosis (Cedarbaum et al., 1999). Subjects with definite or probable laboratory-supported ALS were included in the study. Based on the onset site, patients were classified as having ALS with spinal-onset, bulbar-onset, or spinal/bulbar-onset. Complete neurological evaluation was performed for all patients, classified by the King's staging (Roche et al., 2012) system and the ALSFRS-R (ALS Functional Rating Scale–Revised) score (Paxinos and Watson, 2006; Brooks et al., 2000). Blood from ALS patients was screened for the coding exons of SOD1, ATXN2, and exon 6 of the TARDBP gene. Genomic DNA was amplified by polymerase chain reaction (PCR) and sequenced with the ABI3500xl Genetic Analyzer. FUS was not screened. A repeat-primed polymerase chain reaction assay was used to screen for the presence of the GGGGCC hexanucleotide expansion in the first intron of C9ORF72.

Patients with PD were recruited at the Department of Neurology AO Brotzu, Cagliari, Italy (Supplementary Table S1, PD $n = 5$, HC n = 5). Age and sex-matched healthy individuals were recruited as controls among patient relatives and caregivers.

Samples and data collection was performed in accordance with the Declaration of Helsinki, and received approval of the Sardinian Institutional Research Ethics Committee and ARNAS for PD study (PROT. NP/2023/1562; ARNAS PROT. 355, 03-13-2025), and was conducted in line with the ethical rules for data collection. The informed consent to participate in the study has been obtained from participants.

Table 1
Demographic and clinical features of ALS patients and healthy control subjects.

	ALS (n = 10)	HC (n = 10)
Gender (number)	6F, 4 M	6F, 4 M
Age at sampling (mean ± SD), years	65.4 ± 6.8	57.7 ± 4.8
Age at onset (mean ± SD), years	64.9 ± 6.9	
Clinical signs at onset:		
Spinal	4	
Bulbar	4	
Spinal/Bulbar	2	
King's Stage	1.6 ± 0.8	
ALSFRS-R	39 ± 6.1	
Genetic mutation:		
TARDBP	5	
C9Orf72	2	
No mutation	3	

Data are presented as a mean ± standard deviation (SD). HC = healthy controls; F/M = females/males; ALSFRS = ALS Functional Rating Scale–Revised.

2.3. Power analysis and patients sample size calculation

Sample size estimation for the ALS patient cohort was performed using G*Power 3.1.9.4. The effect size threshold adopted by Liguori et al. (2018) a fold change (FC) > 2, corresponding to $2^{-}\Delta\Delta Cq > 1$ was used as reference. Assuming equal variances between groups, as variance estimates were not reported, and using a two-tailed *t*-test for independent samples, we estimated that 6 cases and 6 controls would provide >80% power to detect differences of $-\log_2(FC) \geq 1$ at a nominal significance level of $P < 0.05$. To account for the nine independent tests included in our validation panel, we also evaluated a multiple-testing–adjusted threshold of $P < 0.005$, which increased the required sample size to 9 cases and 9 controls. Based on these evaluations, a final sample size of 10 cases and 10 controls was selected. (Supplementary Fig. S1).

2.4. Blood collection and PBMC isolation

Blood was collected by standard venipuncture into 7-mL BD Vacutainer® CPT™ tubes (Cat n. 362780 BDA), and PBMC isolation was initiated within 2 h of collection. PBMCs were isolated using Ficoll-Paque density gradient centrifugation at 1800 ×*g* for 30 min at 20 °C. The PBMC layer was aspirated, transferred to a 15-mL Falcon tube, and washed twice with 10 mL PBS. Cells were resuspended in 1 mL PBS and counted using the Scepter™ 2.0 automatic cell counter (Merck Millipore). Cell suspensions were aliquoted into 1.5-mL tubes and centrifuged at 300 ×*g* for 10 min at 20 °C. The supernatant was discarded, and the pellet was resuspended in 200 μL TRIzol and stored at −80 °C until RNA extraction.

2.5. TDP-43 purification

Human FL TDP-43 was cloned, expressed and purified as previously described (Staderini et al., 2022). In brief, *E. coli* cells transformed with the plasmid containing the TDP-43 gene were grown, harvested by centrifugation, lysed by sonication and the resulting suspension was centrifuged to collect the inclusion bodies. These were washed and solubilized at high urea concentration and then loaded onto a HisPur Ni-nitrilotriacetic acid resin gravity flow column. Eluted TDP-43 was refolded by dilution at 4 °C into a well-defined refolding buffer and then subjected at 4 °C to size exclusion chromatography (SEC) and subsequent ion exchange chromatography (AIEX) coupled to an Akta Pure 25 L system using a HiLoad 16/600 Superdex 200 pg column and a HiTrap Q Sepharose Fast Flow 5 mL column, respectively. Purified TDP-43 contained 414 residues plus the N-terminally fused MHHHHHHSSGVDLGTENLYFQS sequence (436 residues in total). Protein quality control was assessed with SDS-PAGE for purity, intrinsic fluorescence for packing and dynamic light scattering for folding, (Supplementary Fig. S2) as previously reported (Staderini et al., 2022; Vivoli Vega et al., 2019; Picotti et al., 2007). The Limulus Amebocyte Lysate (LAL) assay was used to rule out the presence of lipopolysaccharide endotoxins.

2.6. RNA isolation, library preparation and sequencing

Total RNA was extracted using PureLink® RNA Mini Kit (Ambion #12183018 A) according to the manufacturer's instructions. The quantity and integrity of RNA samples were evaluated using Qubit®_2.0 fluorometer and Agilent 2100 Bioanalyzer (Agilent Technologies, Palo Alto, CA, USA). RNA samples showed concentrations ranging from 68 to 90 ng/μL, A260/280 ratios between 1.87 and 1.99 and RNA Integrity Numbers (RIN) between 8.7 and 9.1. RNA-seq libraries were prepared with an Illumina® Stranded mRNA Prep, Ligation Kit (Illumina #20040532) and IDT®_for Illumina®_RNA UD Indexes Set A, Ligation (Illumina #20040553). RNA library concentration and quality were assessed using a Qubit® 2.0 Fluorometer and an Agilent 2100 Bioanalyzer (Agilent Technologies, Palo Alto, CA, USA). The libraries had an average fragment size ranging from 350 to 372 bp and concentrations between 18.6 and 23.2 ng/μL. Sequencing was performed on an Illumina NovaSeq 6000 (Illumina Inc., San Diego, CA, USA).

2.7. Next generation sequencing data processing

Bioinformatic analysis was performed using an in-house developed Snakemake pipeline (https://zenodo.org/records/8369279) to ensure reproducibility and scalability of the analysis workflow. Sequence data (RNA-seq) have been deposited in the NCBIGene Expression Omnibus (GEO) under accession number GSE325171, making the dataset publicly available. Sequence quality control obtained with FastQC and Cutadapt/TrimGalore was inspected in an aggregated interactive report produced through MultiQC. Reads were then aligned to the *Rattus norvegicus* reference genome (Accession ID: GCF_015227675.2) using STAR2. Transcript abundance for each gene and sample was estimated with Kallisto.

2.8. Differential expression analysis

dsDEGs were identified using the DESeq2 R package. (Love et al., 2014). Unsupervised hierarchical clustering was performed using Pearson's correlation and Principal Component Analysis (PCA) was performed to explore the expression variability. Comparisons were conducted between the two study groups (TDP-43-treated vs untreated). Benjamini-Hochberg method was used to adjust DEGs *P* values and a cutoff of FDR < 0.05 was selected as the significant threshold. (Supplementary Excel S.1).

2.9. Reverse transcription quantitative PCR

Total RNA was extracted using the PureLink RNA Mini Kit as described above. First-strand cDNA was synthesized from mRNA using random primers and the SuperScript™ III First-Strand Synthesis System (Cat# 18080–051, Invitrogen), according to the manufacturer's instructions. RT-qPCR was performed using Platinum SYBR Green (Cat# 11744–100, Invitrogen) on an ABI PRISM 7900 Real-Time PCR System (Applied Biosystems, Carlsbad, CA, USA) in 384-well plates. Amplification was carried out over 40 cycles (95 °C for 15 s and 60 °C for 60 s), following an initial incubation at 50 °C for 2 min and denaturation at 95 °C for 10 min.

Expression stability of candidate reference genes was evaluated using geNorm and NormFinder algorithms. GAPDH and β-actin were selected as stable reference genes and normalization was performed using their geometric mean. Gene-specific primers for human and rat targets were designed using Primer3 based on published reference sequences. Primer specificity was verified in silico and primers were commercially synthesized by Eurofins Genomics (Ebersberg, Germany). Primer sequences are provided in Supplementary Table S2.

miRNA expression analysis was performed using the miRCURY LNA Universal RT miRNA PCR system (QIAGEN, Cat# 339340) according to the manufacturer's instructions. RT-qPCR was carried out using the miRCURY SYBR Green PCR Kit (QIAGEN, Cat# 339345) on the ABI PRISM 7900 system under the following conditions: 95 °C for 2 min, followed by 40 cycles of 95 °C for 10 s and 56 °C for 60 s.

All miRNA assays investigated in this study (Supplementary Table S3) were purchased from QIAGEN (hsa-let-7c-3p, hsa-miR-16-5p, hsa-miR-103a-3p, hsa-miR-107, hsa-miR-15b-5p, hsa-miR-195-5p and hsa-miR-328-3p).

hsa-miR-191-5p, hsa-miR-30e-5p, and hsa-miR-30c-5p were identified as the most stable reference miRNAs using NormFinder and geNorm algorithms and were used for normalization based on their geometric mean. All reactions were performed in triplicate and relative gene expression was calculated using the $2^{-}\Delta\Delta Cq$ method (Livak and Schmittgen, 2001). Primer efficiency was assessed using standard

curves generated from serial cDNA dilutions and all primer pairs showed amplification efficiencies between 90.5% and 109%.

2.10. Alternative splicing analysis

Alternative splicing (AS) events were identified and quantified using Replicate Multivariate Analysis of Transcript Splicing (rMATS), version 4.2.0) (Shen et al., 2014) using *Rattus norvegicus* reference genome (Accession ID: GCF_015227675.2). By comparing splicing patterns among experimental groups, various types of splicing events were identified: skipped exons, mutually exclusive exons, 5′ alternative splicing sites, 3′ alternative splicing sites and retained introns. To ensure biological significance of the results, rMATS output was filtered for splicing events with a false discovery rate less than 0.05 and an absolute inclusion level difference (|ΔPSI|) greater than 0.1. These thresholds ensure biological significance defined as a difference of at least 10% in exon inclusion between experimental conditions.

2.11. Identification of miRNAs targeting dsDEGs

miRNA–target gene interactions for dsDEGs in both rats (*Rattus norvegicus*) and humans (*Homo sapiens*) were retrieved using the R package multiMiR (Ru et al., 2014). For rats, all available miRNA interactions were retrieved, whereas for humans only experimentally validated interactions were considered. miRNA sequences were obtained from miRBase, and mature sequences for both rat and human miRNAs were extracted (Ru et al., 2014). To identify conserved miRNAs across species, sequences were compared with a strict criterion of zero mismatches, and common miRNAs were identified. These conserved miRNAs were then cross-referenced with the retrieved miRNA–target interaction data to determine which miRNAs target the same genes in both species. Further validation involved confirming correspondence of miRNA–target interactions in rats and humans. Finally, miRNAs targeting multiple genes were identified, with particular attention to those overlapping among the five genes of interest, providing insight into potential shared regulatory pathways.

2.12. Cell cultures and treatment

The mechanistic link with TDP-43 pathology was further established by analysing the identified gene expression changes in human neuroblastoma cells and healthy donor-derived PBMCs exposed to TDP-43. Human neuroblastoma SH-SY5Y cell line and PBMCs from human healthy donors were cultured respectively in high glucose DMEM and RPMI supplemented with 10% fetal bovine serum, 100 units/mL of penicillin, and 100 μg/mL of streptomycin. SH-SY5Y cells were seeded at a density of 3×10^5 cells/well in 24-well plates and incubated for 24 h with 0.06 μM purified human full-length TDP-43 added to the extracellular medium. PBMCs were plated at the density of 5×10^5 cells/well in 24-well plates and treated for 24 h with 0.1 μM TDP-43 added to the extracellular medium. After TDP-43 incubation, cells were collected, resuspended with TRI Reagent (Sigma-Aldrich, St. Louis, MO) for subsequent molecular biology examinations.

2.13. Statistics

All data are presented as mean ± standard deviation (SD). Statistical significance was assessed by unpaired Student's *t*-test (for two-group comparison), using Prism (GraphPad, USA) version 10.4. *P* values less than or equal to 0.05 were considered statistically significant. $^*p < 0.05$; $^{**}p < 0.01$; $^{***}p < 0.001$.

Receiver operating characteristic (ROC) analyses were performed to assess the ability of each biomarker to discriminate ALS patients from controls. For each gene and miRNA, ROC curves were generated by plotting sensitivity (true positive rate, expressed as a percentage) against 1–specificity (false positive rate, expressed as a percentage) across all possible threshold values. The area under the curve (AUC) was used as a global measure of discriminative performance. We selected cutoff values that maximize Youden's J statistic (J = sensitivity + specificity − 1), which identifies the point on the ROC curve that most effectively balances sensitivity and specificity.

3. Results

3.1. Pathological outcome of FL TDP-43 intracortical infusion in rat

As described elsewhere (Marongiu et al., 2026, bioRxiv, 2026.03.27.714692, doi: https://doi.org/10.64898/2026.03.27.714692), the unilateral infusion of the FL TDP-43 triggered the centrifugal propagation of neuropathology throughout the central nervous system (CNS) and beyond, involving the motor cortex, spinal cord, and skeletal muscles. Intraneuronal phosphorylated TDP-43 (pTDP-43) inclusions were found, together with region-specific neurodegeneration and mitochondrial vulnerability, along the corticospinal axis. In addition, skeletal muscles, specifically the gastrocnemius, exhibited impaired mitochondrial bioenergetics, associated with motor and non-motor behavioral deficits (Marongiu et al., 2026, bioRxiv, 2026.03.27.714692, doi: https://doi.org/10.64898/2026.03.27.714692). These findings demonstrated interneuronal and brain-to-spinal cord-to-muscle propagation of TDP-43 pathology in vivo, establishing a robust non-transgenic model of exogenous FL TDP-43–induced neurotoxicity. Building on evidence of FL TDP-43–induced pathology along the rat corticospinal axis, we aimed to identify a disease-specific (ds) gene expression profile across the same CNS tissues and, ultimately, to validate a corresponding signature in an easily accessible peripheral tissue - such as PBMCs - with diagnostic potential. To this aim, the RNAseq analysis of the primary motor cortex from TDP-43-infused rats was performed, followed by dsDEGs validation using RT-PCR in tissues from the same animal model, including the motor cortex, spinal cord and PBMCs.

3.2. Intracortical infusion of FL TDP-43 induced significant changes in the transcriptional profile of the rat motor cortex

Investigational dsDEGs were identified by RNAseq analysis of motor cortex samples from TDP-43 and vehicle infused rats (TDP-43 $n = 3$, vehicle $n = 4$). Unsupervised hierarchical clustering was produced for the top 10% variable genes (Fig. 2A). PCA showed that samples from vehicle-treated rats were clustered distinctly from samples from TDP-43-treated rats, according to differences of gene expression pattern (Fig. 2B). Differential expression analysis identified, in TDP-43 samples, 5 altered genes affecting biological functions, including 4 upregulated (Mctp1, Penk, Drd1, Rasgrp2) and 1 downregulated gene (Mt2A) compared to vehicle samples (Log2FoldChange > 0; FDR < 0.05), (Fig. 2C). RNA-seq analysis values for dsDEGs between TDP-43 and vehicle samples and respective gene functions are shown in Fig. 2D.

3.3. Cortical dsDEGs were validated across the rat motor cortex, spinal cord and PBMCs

Differential gene expression pattern in the rat motor cortex was further validated by RT-qPCR, confirming the upregulation of mRNA levels for Mctp1, Penk, Drd1, and Rasgrp2 genes, and the downregulation of Mt2A gene (Fig. 3A). Moreover, validation of differential gene expression by RT-qPCR in the cervical spinal cord revealed the same pattern of changes for the five dsDEGs identified in the motor cortex (Fig. 3B). Finally, RT-qPCR analysis of PBMCs from the same rats revealed the same expression pattern of the five dsDEGs identified in the cortex and spinal cord (Fig. 3C), indicating that PBMCs mirror the molecular alterations occurring in TDP-43–affected nervous tissues.

To further confirm that the observed gene expression changes were specifically induced by TDP-43, we performed the same RT-qPCR

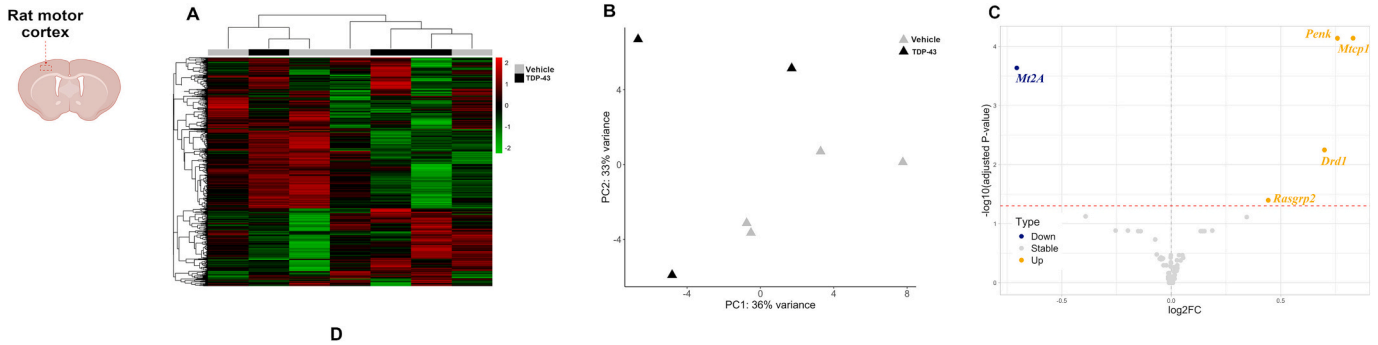

D

Gene	Gene name	Log2 Fold change	P-value	Adjusted p-value	Gene function
Mctp1	Multiple C2 and transmembrane domain containing 1 [Source:RGD Symbol;Acc:1305199]	0.83	5.5e-09	0.000072	Mctp1 gene enables calcium ion binding activity. Predicted to be involved in several processes, including modulation of chemical synaptic transmission, negative regulation of endocytosis and negative regulation of response to oxidative stress.
Penk	Proenkephalin [Source:RGD Symbol;Acc:68946]	0.76	8.2e-09	0.000072	Penk gene encodes a preproprotein that is proteolytically processed to generate multiple protein products that include pentapeptide opioids Met-enkephalin and Leu-enkephalin.
Mt2A	Metallothionein 2A [Source:RGD Symbol;Acc:15923453]	-0.71	3.9e-08	0.00023	Mt2A gene regulates metal homeostasis, detoxification, oxidative stress, immune defense, cell cycle progression, cell proliferation and differentiation and angiogenesis.
Drd1	Dopamine receptor D1 [Source:RGD Symbol;Acc:2518]	0.7	1.3e-06	0.0056	Drd1 gene encodes the D1 subtype of the dopamine receptor, the most abundant dopamine receptor in the central nervous system. The dopamine acts as an important regulator of immune function and affects the oxidative metabolism of peripheral blood lymphocytes through the D1 receptor, resulting in reduced ROS production.
Rasgrp2	RAS guanyl releasing protein 2 [Source:RGD Symbol;Acc:1311630]	0.44	0.00011	0.04	Rasgrp2 gene encode a brain-enriched nucleotide exchanged factor that contains an N-terminal GEF domain, 2 tandem repeats of EF-hand calcium-binding motifs, and a C-terminal diacylglycerol/phorbol ester-binding domain.

Fig. 2. Gene expression pattern in rat motor cortex. (A) Heatmap visualizing the gene expression profiles derived from 7 distinct transcriptomic analyses of the rat motor cortex (3 TDP-43 and 4 vehicles). Genes are reported in rows, samples in columns. The relative up and down regulation of genes is indicated by red and green, respectively. Unsupervised hierarchical clustering analysis was performed using the top 10% most variable genes. Dendrograms of clustering analysis for samples and genes are displayed on the top and left, respectively, showing gene expression profiles. (B) Principal Component Analysis of DEGs variance. PCA shows the 7 samples, including those treated with vehicle (grey) and TDP-43 (black). Each dot indicates one sample. (C) Volcano plot displaying transcriptional expression levels of all analyzed genes, integrating both statistical significance and magnitude of change. Data points represent individual genes: blue, yellow and grey indicate significantly downregulated, upregulated and unchanged transcripts, respectively, compared to vehicle-treated samples. The horizontal dashed grey line indicates the significance threshold ($-\log_{10}$ (p-value), with $p < 0.05$). The plot was generated using the ggplot2 package in R. (D) Description of dsDEGs identified by differential expression analysis in the rat motor cortex. Values and biological characteristics of upregulated (Mctp1, Penk, Drd1, Rasgrp2) and downregulated (Mt2A) genes are shown. Adjusted p-values were made using the Benjamini-Hochberg method. Summaries for all genes were retrieved from GeneCards - The Human Gene Database. (For interpretation of the references to colour in this figure legend, the reader is referred to the web version of this article.)

analysis on cortical tissue from rats infused with a control protein (toxic α-synuclein oligomers). Notably, the transcriptional alterations detected following TDP-43 infusion were not observed in the cortex of α-synuclein–infused rats, indicating that these gene expression changes are specific to TDP-43. (Supplementary Fig. S3).

3.4. dsDEGs were also identified in PBMCs from individuals diagnosed with ALS

Comparative analysis using the Ensembl database confirmed that the five dsD EGs under investigation are highly conserved between rats and humans. Therefore, to assess their translational relevance, the expression of these TDP-43–associated dsDEGs was evaluated in PBMCs from 10 individuals with ALS and 10 healthy controls (HCs). Demographic, clinical and genetic features of ALS patients and HCs are reported in Table 1. PBMCs from ALS patients and HCs were analyzed by RT-qPCR (Fig. 4A), revealing significant dysregulation of all five dsDEGs under investigation. Interestingly, while some dsDEGs exhibited changes in the same direction as those observed in rats, others showed opposite trends, which may reflect differences in disease stage in human pathology or species-related factors. Specifically, the mRNA levels of Mctp1, with a fold change of 1.58 ± 0.1 ($P = 1.4E-05$), and Drd1, with a fold change of 2.29 ± 0.1 ($P = 0.0003$), were significantly upregulated, whereas those of Penk, with a fold change of 0.48 ± 0.02 ($P = 0.004$), Mt2A with a fold change of 0.37 ± 0.03 ($P = 0.0009$), and Rasgrp2 with a fold change of 0.57 ± 0.03 ($P = 1.5E-05$), were markedly downregulated.

To assess the ALS-specificity of these transcriptional changes, the expression of the same five dsDEGs was evaluated by RT-qPCR in PBMCs from a small cohort of PD patients ($n = 5$) and age-matched controls (n = 5) (Supplementary Fig. S4, Supplementary Table S1). None of the five genes exhibited a comparable pattern of dysregulation in this cohort, indicating that the identified gene set is likely specific to ALS rather than representing general markers of neurodegeneration.

3.5. Exposure to FL TDP-43 modulated the expression of the dsDEGs in human neuroblastoma cells and PBMCs from healthy donors

To confirm the causal role of FL TDP-43 in modulating dsDEG expression, cultured human neuroblastoma SH-SY5Y cells and PBMCs from healthy donors were treated with FL TDP-43. The results demonstrated that TDP-43 significantly altered the expression of these genes, with partially consistent trends observed across both cell types. Specifically, Mctp1 and Drd1 were upregulated, whereas Penk and Mt2A were downregulated in both cell types compared to vehicle-treated controls (Fig. 4B–C). Rasgrp2 was downregulated in TDP-43–treated PBMCs but showed no significant change in neuroblastoma cells. These findings indicate a context-dependent effect of TDP-43 on the transcriptional regulation of selected target genes. Notably, the observed dsDEG regulation in TDP-43–treated PBMCs closely mirrored the patterns seen in PBMCs from ALS patients, supporting the conclusion that these changes are specifically driven by extracellular TDP-43.

3.6. Identification of miRNAs targeting dsDEGs

miRNAs and alternative splicing are significantly involved in ALS pathophysiology (Alkhazaali-Ali et al., 2024; Friedman et al., 2009; Freischmidt et al., 2015). Here, computational analysis identified seven conserved miRNAs in both rats and humans that target the identified DEGs. Specifically, hsa-miR-107 (corresponding in rats to rno-miR-107-3p), hsa-miR-15b-5p (rno-miR-15b-5p), hsa-miR-16-5p (rno-miR-16-

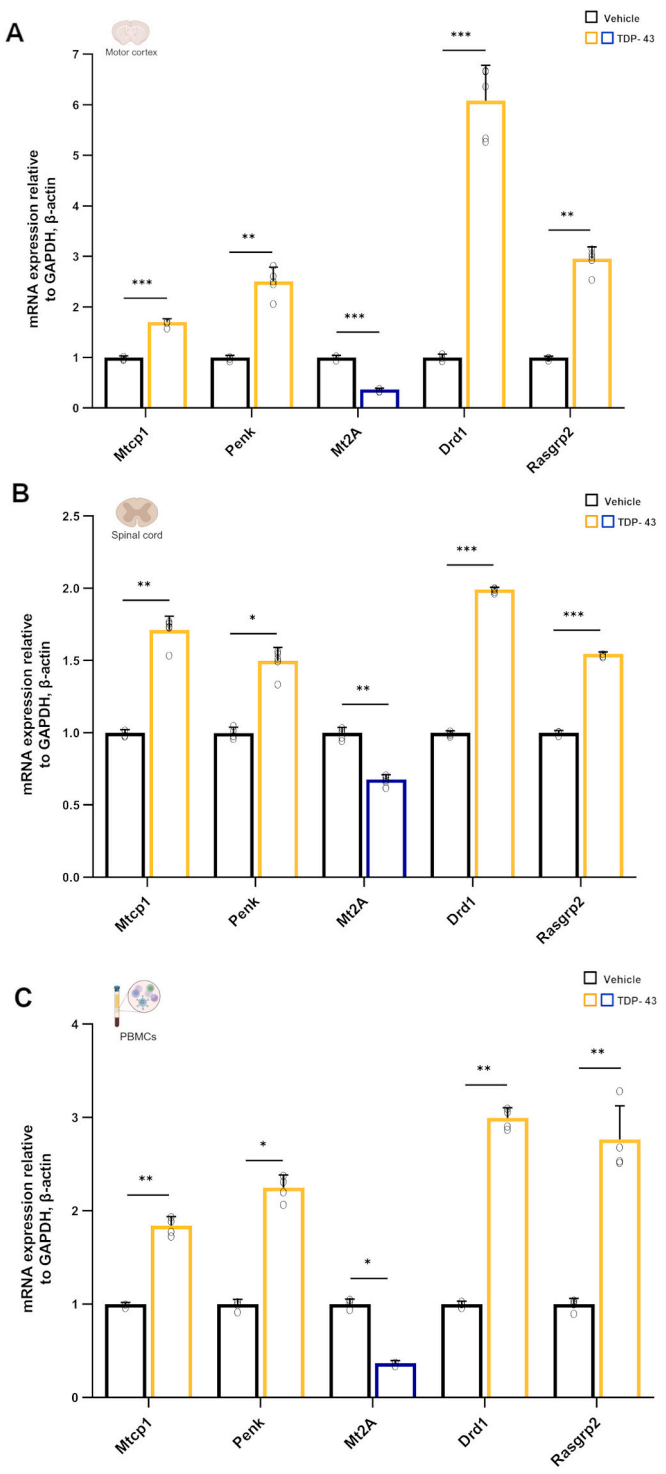

Fig. 3. Maintenance of 5 dsDEGs pattern across the rat nervous tissues and PBMCs. mRNA expression analysis of Mctp1, Penk, Mt2A, Drd1 and Rasgrp2 genes in the motor cortex (TDP-43 $n = 4$; vehicle $n = 5$) (A), cervical spinal cord (TDP-43 n = 5 vehicle n = 5) (B) and PBMCs (TDP-43 n = 4; vehicle n = 4) (C) of TDP-43 and vehicle injected rats. Blue and yellow indicate significantly downregulated and upregulated genes, respectively, compared to vehicle-treated samples. Statistical significance was determined using a *t*-test, with significance levels indicated as follows: *p < 0.05, **$p < 0.01$ and ***$p < 0.001$. All reactions were performed in triplicate and relative gene expression was calculated using the $2^{-}\Delta\Delta$Cq method. Data are shown as mean ± standard deviation (SD); error bars indicate SD. (For interpretation of the references to colour in this figure legend, the reader is referred to the web version of this article.)

5p), hsa-miR-103a-3p (rno-miR-103-3p), and hsa-miR-195-5p (rno-miR-195-5p) target both Penk and Drd1, while hsa-miR-328-3p (rno-miR-328-3p) targets both Drd1 and Rasgrp2, and hsa-let-7c-3p (rno-let-7c-1-3p) regulates both Mt2A and Rasgrp2 (Fig. 5A). Instead, the alternative splicing analysis of the rat dsDEGs revealed no significant dysregulation.

RT-qPCR comparative analysis between PBMCs from ALS and HCs revealed a significant downregulation of four out of the seven selected miRNAs in ALS ($p < 0.05$). Specifically, miR-15b-5p (fold change 0.45 ± 0.04, $P = 0.0004$), miR-16-5p (fold change 0.34 ± 0.02, $P = 4.7E-05$), miR-103a-3p (fold change 0.38 ± 0.02, $P = 1.4E-05$) and miR-195-5p (fold change 0.31 ± 0.03, $P = 3.1E-06$), showed significant reduced expression levels (Fig. 5B).

3.7. Diagnostic performance in ALS of dsDEGs and related miRNAs from PBMCs

The diagnostic performance of dsDEGs and their associated miRNAs identified in PBMCs was evaluated using receiver operating characteristic (ROC) curve analysis, with the area under the curve (AUC) providing a comprehensive measure of each biomarker's ability to discriminate between ALS patients and healthy controls (HCs) across all classification thresholds. Among the dsDEGs, Penk showed good discrimination (AUC = 0.87; cutoff $< 1.370 \times 10^{-4}$; sensitivity = 90%, specificity = 80%), while Drd1, Rasgrp2 and Mt2A displayed excellent accuracy (AUCs = 0.94–0.98) (Fig. 6 A-E). Specifically, Drd1 (cutoff $> 1.705 \times 10^{-4}$) reached 100% sensitivity and 90% specificity; Rasgrp2 (cutoff $< 5.389 \times 10^{-2}$) showed 100% sensitivity and 90% specificity; and Mt2A (cutoff $< 2.970 \times 10^{-3}$) achieved 100% sensitivity and 80% specificity. Notably, Mctp1 (cutoff $> 1.053 \times 10^{-1}$) reached perfect discrimination, with both sensitivity and specificity of 100%.

Similarly, miRNAs exhibited very high discriminative performance (Fig. 7 A-D). miR-15b-5p (cutoff $< 3.286 \times 10^{1}$) reached an AUC of 1.00 with 100% sensitivity and specificity, while miR-16-5p (cutoff $< 1.810 \times 10^{2}$), miR-103a-3p (cutoff $< 1.407 \times 10^{2}$) and miR-195-5p (cutoff $< 2.191 \times 10^{-2}$) all showed excellent accuracy (AUCs > 0.95), with sensitivities of 100% and specificities of 80%, 90% and 90%, respectively. Collectively, these results demonstrate the exceptional discriminative capacity and high diagnostic accuracy of dsDEGs and their associated miRNAs in PBMCs, highlighting their strong potential as robust, non-invasive biomarkers for ALS diagnosis.

4. Discussion

A major challenge in ALS research is the identification of biomarkers that are both disease-specific and capable of detecting the condition at an early stage. Numerous molecular candidates measurable in biofluids, as well as in skin or muscle biopsies, have been proposed. While many of these markers show prognostic value, they often lack sufficient specificity and sensitivity for early diagnosis. These include indicators of blood–brain barrier disruption (e.g., metalloproteinases), axonal degeneration (e.g., neurofilament chains and Tau protein), TDP-43 pathology, and markers of inflammation or oxidative stress (Belbasis, 2025; Riva et al., 2022; Rossi et al., 2018; Staats et al., 2022; Sturmey and Malaspina, 2022). Although high-throughput gene expression profiling of peripheral blood has significantly expanded the repertoire of candidate circulating biomarkers, the complex and multisystem nature of ALS continues to hinder the identification of disease-specific molecular signatures (Dragoni et al., 2025; Liguori et al., 2018).

4.1. From brain to blood: peripheral detection of TDP-43-induced DEGs in the TDP-43 rat model

In this study, we developed a translational strategy to identify transcriptional changes in PBMCs from ALS patients that are specifically linked to TDP-43 toxicity and therefore reflect the underlying

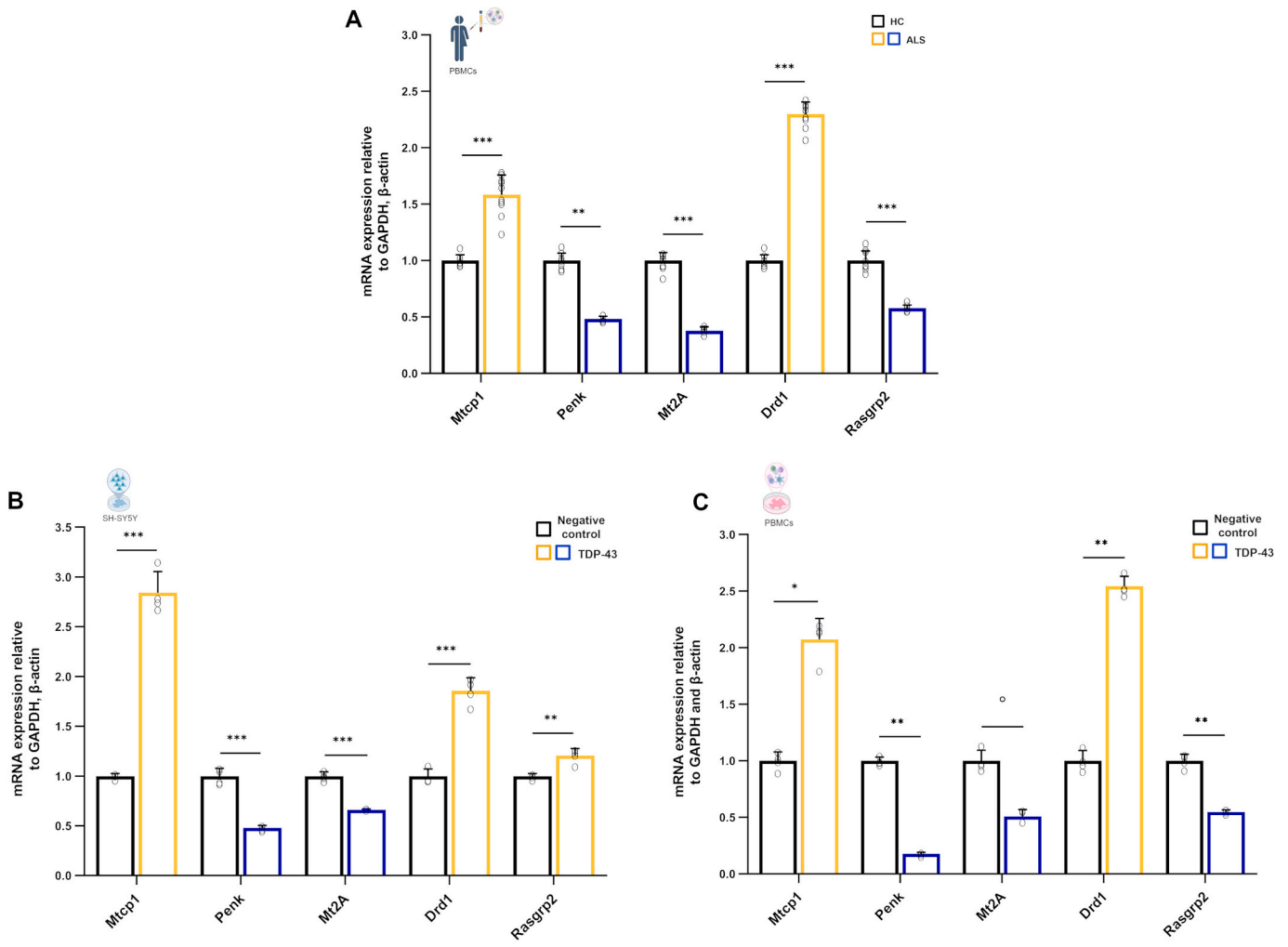

Fig. 4. dsDEGs in PBMCs from ALS individuals relative to HCs and modulation of dsDEGs expression by TDP-43 in human neuroblastoma cells and human PBMCs. (A) Relative mRNA expression analysis of Mctp1, Penk, Mt2A, Drd1 and Rasgrp2 genes in PBMCs of ALS patients and HCs. Each group includes $n = 10$ participants. Blue and yellow indicate significantly downregulated and upregulated genes, respectively, compared to HCs. mRNA expression analysis of Mctp1, Penk, Mt2A, Drd1 and Rasgrp2 genes in human neuroblastoma SH-SY5Y cells (B) and PBMCs from healthy human donors (C) following TDP-43 treatment. SH-SY5Y cells and PBMCs TDP-43, n = 4; vehicle, *n = 4. In line with the directional hypothesis developed in* Fig. 4A, a one-tailed test was applied in Fig.4C. A *$p < 0.10$ was considered suggestive and indicated by '°'. Blue and yellow indicate significantly downregulated and upregulated genes, respectively, compared to vehicles. Statistical significance was determined using a t-test, with significance levels indicated as follows: **$p < 0.01$ and ***$p < 0.001$. All reactions were performed in triplicate and relative gene expression was calculated using the* $2^{-\Delta\Delta Cq}$ method. Data are shown as mean ± standard deviation (SD); error bars indicate SD. (For interpretation of the references to colour in this figure legend, the reader is referred to the web version of this article.)

neuropathology. This approach builds on a recent preclinical model in which a single intracerebral infusion of FL human TDP-43 into the rat primary motor cortex induced an ALS-like proteinopathy (Marongiu et al., 2026, bioRxiv, 2026.03.27.714692, doi:https://doi.org/10.64898/2026.03.27.714692). Four months post-infusion, intraneuronal pTDP-43 inclusions were found in the motor cortex and in the cervical spinal cord, along with mitochondrial alterations and region-specific neurodegeneration. In addition, impaired mitochondrial bioenergetics were detected in the gastrocnemius muscle, together with motor and non-motor behavioral deficits (Marongiu et al., 2026, bioRxiv, 2026.03.27.714692, doi:https://doi.org/10.64898/2026.03.27.714692).

Using this rat model and applying stringent selection criteria (top 10% most variable genes, FDR < 0.05), we identified five differentially expressed genes (DEGs) in cortical tissue. Importantly, these DEGs were consistently detected across the motor cortex, spinal cord, and peripheral PBMCs. This result aligns with the pathological findings described in the model and indicate that TDP-43 pathology triggers a coordinated transcriptional response across central and peripheral compartments. This cross-tissue overlap supports the existence of a disease-relevant molecular program and provides a strong proof-of-concept for the clinical translatability of our findings.

The identification of TDP-43-induced DEGs is consistent with the established role of TDP-43 pathology in ALS. TDP-43-positive inclusions are observed in the majority of ALS cases, both sporadic and familial, highlighting its central role as a shared pathological hallmark (Mackenzie et al., 2007). Cytoplasmic pTDP-43 aggregates have been detected in cortical and hippocampal neurons, as well as in motor neurons (Neumann et al., 2006; Riva et al., 2022). Moreover, preclinical models, including transgenic mice and viral vector-based rat models, have demonstrated that TDP-43 mislocalization and aggregation can recapitulate key features of ALS pathology, including neurodegeneration along the cortico-motoneuronal axis (Dance, 2010; Wang et al., 2011; Reale et al., 2023). Collectively, this evidence supports the relevance of TDP-43-driven transcriptional changes as candidate biomarkers of ALS neuropathology.

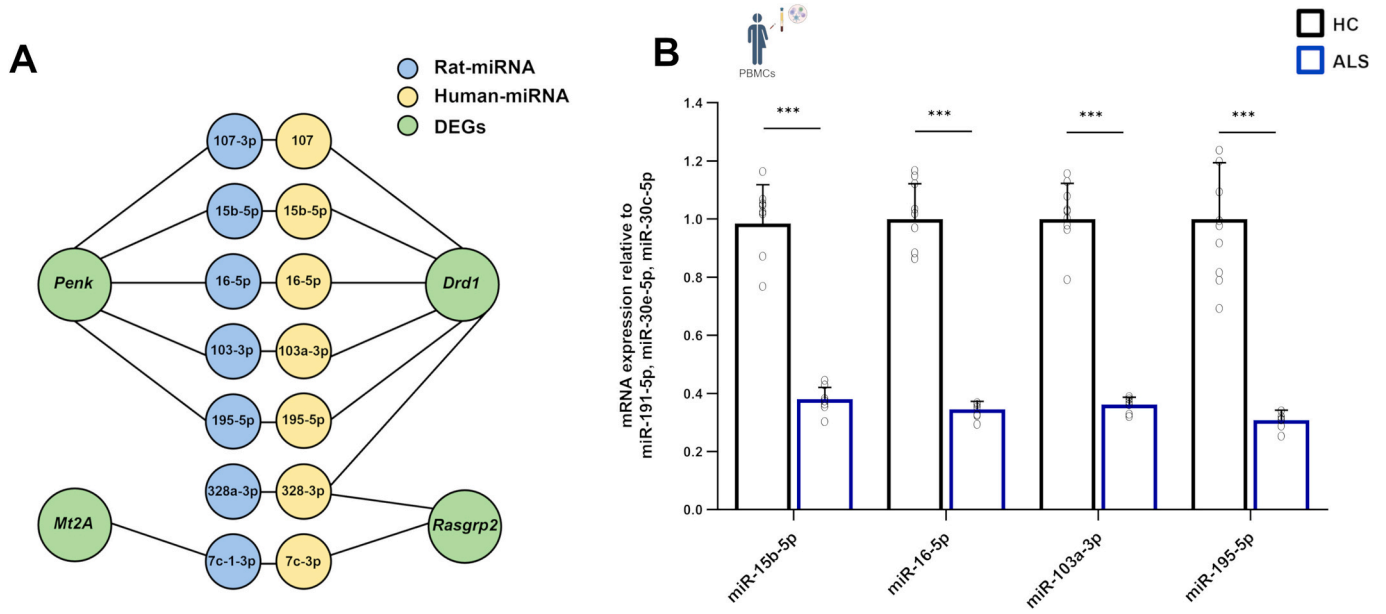

Fig. 5. Dysregulation of miRNA expression in human PBMCs from ALS cases. (A) miRNA-target genes network. Extended names of miRNAs in rats and humans are prefixed with *rno* and *hsa*, respectively. (B) Relative miRNAs expression in human PBMCs from ALS cases and HCs. Each group includes n = 10 participants, statistical significance was determined using a t-test, with significance levels indicated ***$p < 0.001$. All reactions were performed in triplicate and relative gene expression was calculated using the $2^{-}\Delta\Delta Cq$ method. Data are shown as mean ± standard deviation (SD); error bars indicate SD.

4.2. Validation of dsDEGs in ALS patient-derived PBMCs

Applying our translational approach, we detected the same dsDEGs identified in the preclinical model in PBMCs from ALS patients, but not in healthy controls. Previous studies have reported pathological alterations in PBMCs from ALS patients, including TDP-43 cytoplasmic mislocalization and protein expression changes, supporting their potential diagnostic relevance (De Marco et al., 2017; Filareti et al., 2017; Mosallaei et al., 2022; Nardo et al., 2011; Yu et al., 2025). Here, we extend these observations by identifying a distinct PBMC gene expression signature (dsDEGs) that mirrors TDP-43-driven toxicity in the nervous system.

Notably, the direct involvement of TDP-43 in regulating these genes was further supported by in vitro experiments, where exposure of healthy PBMCs to exogenous FL TDP-43 reproduced the same expression patterns observed in ALS-derived PBMCs. Importantly, these gene expression changes were not observed in PBMCs from patients with PD, supporting their disease specificity.

While the 5 dsDEGs identified in the preclinical model were all dysregulated in ALS PBMCs, three of them, namely Mctp1, Mt2A and Drd1 also displayed the same direction across animal and human tissues, suggesting that they more closely reflect the nervous system pathology. These dsDEGs have been only marginally explored in ALS. However, their known biological functions suggest their relevance to disease mechanisms and strongly suggest that their altered expression in PBMCs reflects the nervous system pathology.

Mctp1 is involved in AKT signaling, a pathway previously reported to be dysregulated in ALS (Laine et al., 2002). Our finding of Mctp1 overexpression in ALS PBMCs aligns with AKT hyperphosphorylation described in the ALS spinal cord (Hu et al., 2003) and may play a role in the pathological phosphorylation and aggregation of TDP-43. Of note, this gene was consistently upregulated in the nervous tissue of our animal model displaying phosphorylated TDP-43 aggregates, supporting its pathological role. Therefore, increased Mctp1 expression in ALS PBMC may be interpreted as a biomarker on nervous system pathology.

Mt2A was consistently downregulated across tissues in our study, in line with previous studies reporting decreased levels in the spinal cord of ALS patients (Hozumi et al., 2008). Mt2A has been associated with neuroprotection, and its deficiency has been shown to exacerbate disease progression in ALS models (Puttaparthi et al., 2002). More recently, metalloprotein 3 (Mt3) expression was also found significantly decreased in the spinal cord of ALS patients (Gunn et al., 2026) As part of brain barriers, Mt. levels are generally dysregulated early in pathological brain states (Jakovac et al., 2013). Therefore, our results align with a pathological outcome of Mt2A downregulation and support the decreased expression in PBMCs as a biomarker of the nervous system pathology.

Drd1, encoding the dopamine D1 receptor, is particularly interesting given the role of dopamine in modulating immune responses and oxidative stress in peripheral lymphocytes (Matt et al., 2020). Of note, spinal cord astrocytes are highly sensitive to local dopamine and noradrenaline alterations (Montalant et al., 2024) providing a mechanistic ground for the pathological involvement of D1R alterations in ALS pathogenesis (Wu et al., 2020).

4.3. MicroRNAs targeting dsDEGs

We further identified 7 miRNAs targeting the identified dsDEGs, four of which – miR-15b-5p, miR-16-5p, miR-103a-3p, miR-195-5p - were significantly downregulated in PBMCs from ALS patients. Consistent with our findings, similar miRNA alterations have been reported in sporadic ALS (Liguori et al., 2018), and Drd1 has been validated as a target of miR-15b-5p and miR-16-5p (Wu et al., 2020). miRNAs are particularly attractive biomarkers in neurodegenerative diseases due to their role in post-transcriptional gene regulation and their stability in biofluids. Importantly, TDP-43 itself is a key regulator of RNA metabolism, including miRNA biogenesis and splicing (Buratti et al., 2010). Dysregulation of miRNAs has been widely reported in ALS across multiple tissues and biofluids, including CSF, serum, spinal cord and blood leukocytes, often correlating with disease progression. This supports their dual role as both mechanistic contributors to disease and potential early diagnostic markers (Freischmidt et al., 2015; Liguori et al., 2018).

4.4. Diagnostic potential of dsDEGs and related miRNAs

ROC curve analyses based on RT-qPCR data demonstrated a strong

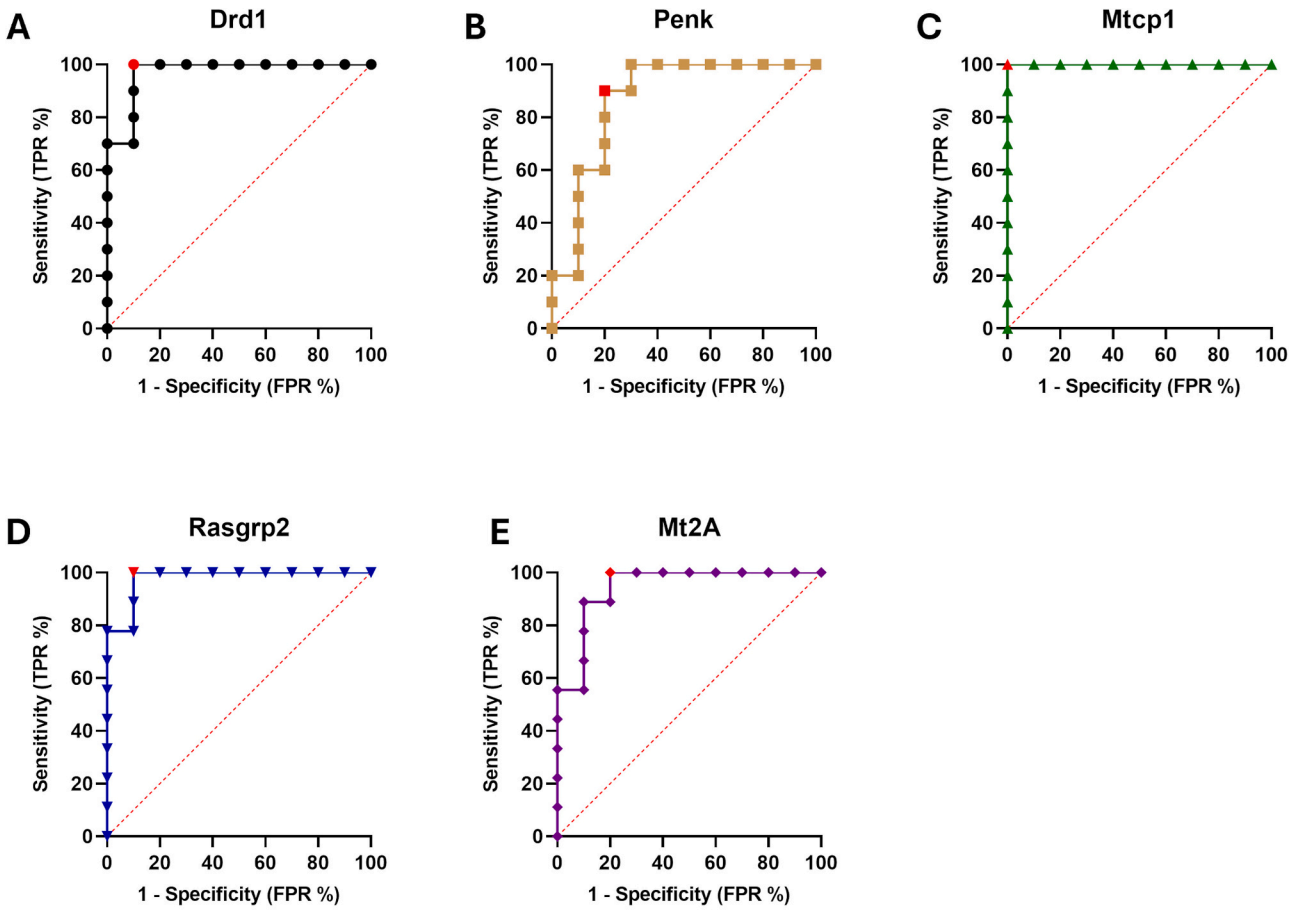

dsDEGs	AUC	SE	95% CI	p value	Cut-off value ($2^{-\Delta Ct}$)	Sensitivity% (95% CI)	Specificity% (95% CI)	Likelihood ratio	Youden Index
Penk	0.870	0.0873	0.67 to 1.00	0.0052	$> 1.705 \times 10^{-4}$	100 (72.25% to 100%)	90 (59.58% to 99.49%)	10	0.90
Drd1	0.970	0.0347	0.90 to 1.00	0.0004	$< 1.370 \times 10^{-4}$	90 (59.58% to 99.49%)	80 (49.02% to 96.45%)	4.5	0.70
Mtcp1	1.000	0.000	1.00 to 1.00	0.0002	$> 1.053 \times 10^{-1}$	100 (72.25% to 100.0%)	100 (72.25% to 100.0%)	-	1
Rasgrp2	0.978	0.0284	0.92 to 1.00	0.0004	$< 5.389 \times 10^{-2}$	100 (70.09% to 100.0%)	90 (59.58% to 99.49%)	10	0.9
Mt2A	0.944	0.0514	0.84 to 1.00	0.0011	$< 2.970 \times 10^{-3}$	100 (70.09% to 100.0%)	80 (49.02% to 96.45%)	5	0.8

Fig. 6. Diagnostic performance in ALS of dsDEGs and related miRNAs from PBMCs. ROC curves for the dsDEGs (A) Drd1, (B) Penk, (C) Mctp1, (D) Rasgrp2, and (E) Mt2A quantified in PBMCs by RT-qPCR. For each biomarker, the ROC curve shows sensitivity (true positive rate (TPR), expressed as a percentage) plotted against 1–specificity (false positive rate (FPR), expressed as a percentage) across all possible cutoff values. The red marker on each curve indicates the optimal cutoff identified using Youden's Index. The tables below report, for each dsDEG, the AUC, standard error, 95% CI, p-values, optimal cutoff, sensitivity (%), specificity (%), likelihood ratios, and Youden's index. Abbreviations: AUC, area under the curve; CI, confidence interval; dsDEGs, disease-specific differentially expressed genes. (For interpretation of the references to colour in this figure legend, the reader is referred to the web version of this article.)

discriminative ability of both dsDEGs and their associated miRNAs in PBMCs, with all biomarkers showing AUC values above 0.8. Notably, Mctp1 and miR-15b-5p achieved perfect discrimination (AUC = 1.00), supported by optimal cutoff values and a Youden index of 1. dsDEGs were not detected in PBMCs from a small cohort of PD patients. If validated in a larger cohort of PD and other neurodegenerative disorders, these PBMC-based results would further strengthen the evidence for the disease specificity of the identified biomarkers.

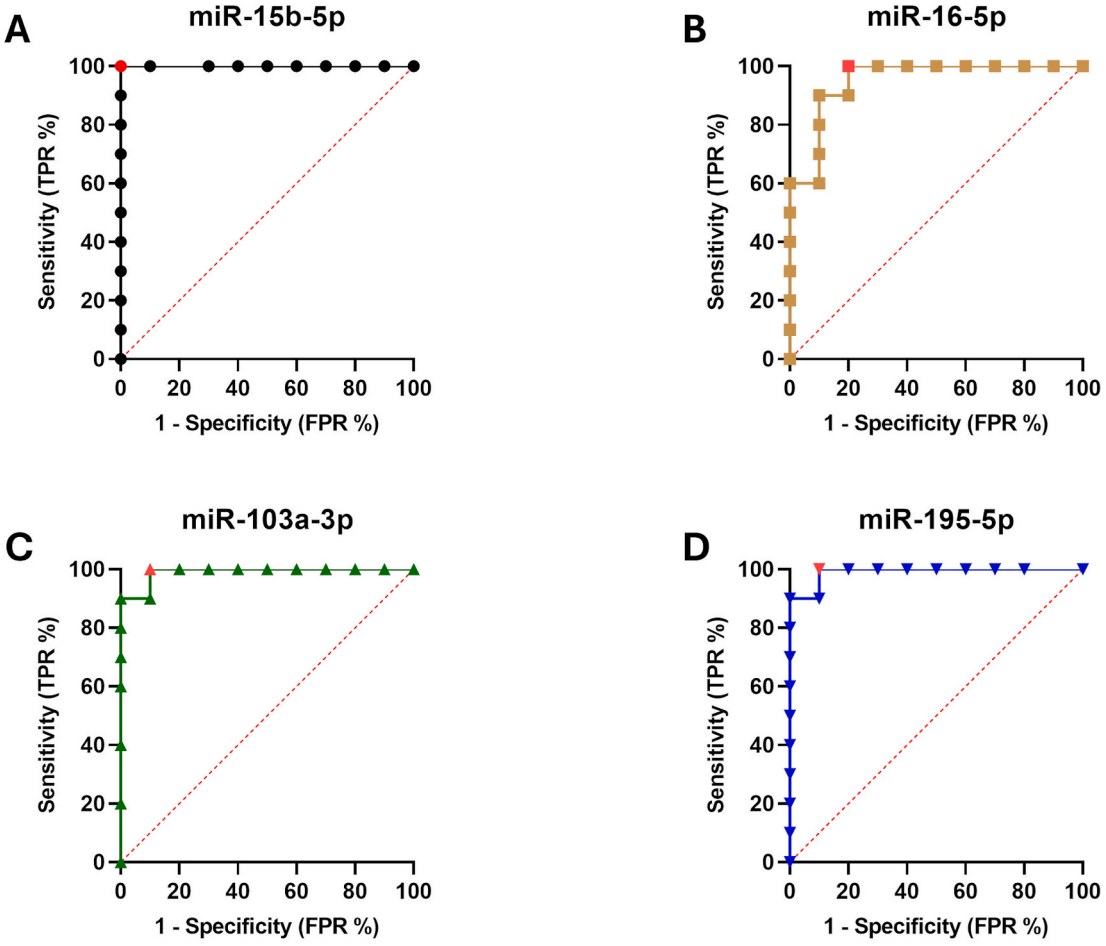

dsDEGs	AUC	SE	95% CI	p value	Cut-off value ($2^{-\Delta Ct}$)	Sensitivity% (95% CI)	Specificity% (95% CI)	Likelihood ratio	Youden Index
miR-15b-5p	1.000	0.0000	1.00 to 1.00	0.0002	< 32.86	100 (72.25% to 100.0%)	100 (72.25% to 100.0%)	-	1
miR-16-5p	0.950	0.0467	0.86 to 1.00	0.0007	< 181.0	100 (72.25% to 100.0%)	80 (49.02% to 96.45%)	5	0.8
miR-103a-3p	0.990	0.0161	0.96 to 1.00	0.0002	< 140.7	100 (72.25% to 100.0%)	90 (59.58% to 99.49%)	10	0.9
miR-195-5p	0.990	0.0161	0.96 to 1.00	0.0002	< 0.0219	100 (72.25% to 100.0%)	90 (59.58% to 99.49%)	10	0.9

Fig. 7. Diagnostic performance of miRNAs in PBMCs from ALS patients. ROC curves for the miRNAs (A) miR-15b-5p, (B) miR-16-5p, (C) miR-103a-3p, and (D) miR-195-5p quantified in PBMCs by RT-qPCR. For each biomarker, the ROC curve shows sensitivity (true positive rate (TPR), expressed as a percentage) plotted against 1–specificity (false positive rate (FPR), expressed as a percentage) across all possible cutoff values. The red marker on each curve indicates the optimal cutoff identified using Youden's Index. The tables below report, for each miRNA, the AUC, standard error, 95% CI, p-values, optimal cutoff, sensitivity (%), specificity (%), likelihood ratios, and Youden's index. Abbreviations: AUC, area under the curve; CI, confidence interval. (For interpretation of the references to colour in this figure legend, the reader is referred to the web version of this article.)

Despite the limited cohort size (10 ALS patients and 10 controls) of this pilot study, the identified biomarkers were consistently detectable across both sexes and at relatively early disease stages (ALSFRS-R: 28–46; King's stage: 1–4a at the time of PBMCs collection). This is particularly relevant given the well-known diagnostic delay in ALS, which often results in significant disease progression before clinical diagnosis.

None of the patients in this cohort carried SOD1 mutations, in line

with the limited frequency of this mutation, particularly in sardinian ALS patients and according to the pilot nature of our study. Therefore, the applicability of these findings to specific genetic subtypes such as SOD1 mutations remains to be established. Future studies in larger, sex-balanced cohorts, including individuals from external validation cohorts with diverse genetic backgrounds and geographical origin, will be essential to validate these findings and assess the biomarker performance in a more heterogeneous ALS population.

5. Conclusion

Using a translational approach, we identified a novel ALS-specific dsDEG/miRNA signature driven by CNS TDP-43 pathology, which propagates from affected neural tissues to peripheral PBMCs. In a pilot cohort of ALS patients, this signature exhibited strong discriminative power and high sensitivity, supporting its potential as a robust diagnostic biomarker for ALS. Overall, the present work, by addressing the unmet need in ALS of minimally invasive, disease-specific diagnostic biomarkers is highly significant and provides a substantial level of advancement as a pilot translational study. By linking central TDP-43 pathology with a detectable PBMC gene–miRNA signature, our work provides a blood-based biomarker with potential international relevance and global perspective for a worldwide disease such as ALS.

CRediT authorship contribution statement

Maria Francesca Manchinu: Writing – original draft, Supervision, Project administration, Investigation, Funding acquisition, Conceptualization. **Michela Congiu:** Validation, Software, Methodology, Investigation. **Matteo Massidda:** Writing – original draft, Software, Investigation, Formal analysis, Data curation. **Giuseppe Borghero:** Writing – original draft, Resources, Methodology. **Jacopo Marongiu:** Methodology. **Isabella Marzi:** Methodology. **Andrea Maschio:** Validation, Software, Methodology, Investigation. **Vincenzo Rallo:** Validation, Software, Methodology, Investigation. **Marcello Serra:** Writing – original draft, Software, Investigation, Formal analysis, Data curation. **Clara Porcedda:** Methodology. **Michela Etzi:** Methodology. **Maria Francesca Palmas:** Methodology. **Andrea Angius:** Writing – original draft, Software, Investigation, Formal analysis, Data curation. **Valeria Sogos:** Methodology. **Maria Ida Pateri:** Methodology. **Maristella Steri:** Writing – original draft, Software, Investigation, Formal analysis, Data curation. **Valentina Coroneo:** Methodology. **Alfonso De Simone:** Methodology. **Giovanni Cossu:** Resources, Methodology. **Fabrizio Chiti:** Writing – review & editing, Funding acquisition. **Anna Rosa Carta:** Writing – review & editing, Supervision, Funding acquisition, Conceptualization.

Funding

This study was supported by Prin 2020 grant N 2020PBS5MJ; Fondazione di Sardegna grant N 2025-0088.

Declaration of competing interest

The authors report no competing interests.

Acknowledgements

We acknowledge Cesast (Academic Services Center for Animal Facility) for animal care and housing, and Cesar (Academic Services Center for Research Support) for technical assistance at the University of Cagliari.

Appendix A. Supplementary data

Supplementary data to this article can be found online at https://doi.org/10.1016/j.nbd.2026.107473.

Data availability

Data will be made available on request.

References

Alkhazaali-Ali, Z., et al., 2024. MicroRNA (miRNA) as a biomarker for diagnosis, prognosis, and therapeutics molecules in neurodegenerative disease. Biomed. Pharmacother. 177, 116899. https://doi.org/10.1016/j.biopha.2024.116899.

Belbasis, L., et al., 2025. Mendelian randomization identifies proteins involved in neurodegenerative diseases. Brain. https://doi.org/10.1093/brain/awaf018 awaf018.

Brettschneider, J., et al., 2013. Drug therapy for pain in amyotrophic lateral sclerosis or motor neuron disease. Cochrane Database Syst. Rev. (6), CD005226. https://doi.org/10.1002/14651858.CD005226.pub3.

Brooks, B.R., World Federation of Neurology Research Group on Motor Neuron Diseases, et al., 2000. El Escorial revisited: revised criteria for the diagnosis of amyotrophic lateral sclerosis. Amyotroph. Lateral Scler. Other Motor Neuron Disord. 1 (5), 293–299. https://doi.org/10.1080/146608200300079536.

Buratti, E., et al., 2010. Nuclear factor TDP-43 can affect selected microRNA levels. FEBS J. 277 (10), 2268–2281. https://doi.org/10.1111/j.1742-4658.2010.07643.x.

Cedarbaum, J.M., et al., 1999. The ALSFRS-R: a revised ALS functional rating scale that incorporates assessments of respiratory function. BDNF ALS Study Group (Phase III). J. Neurol. Sci. 169 (1–2), 13–21. https://doi.org/10.1016/s0022-510x(99)00210-5.

Chiò, A., et al., 2011. Large proportion of amyotrophic lateral sclerosis cases in Sardinia due to a single founder mutation of the TARDBP gene. Arch. Neurol. 68 (5), 594–598. https://doi.org/10.1001/archneurol.2010.352.

Dance, A., 2010. TDP-43 models coverage. J. Alzheimer's Dis 21 (4), 1403–1408. https://doi.org/10.3233/JAD-2010-101543.

De Marco, G., et al., 2017. Monocytes of patients with amyotrophic lateral sclerosis linked to gene mutations display altered TDP-43 subcellular distribution. Neuropathol. Appl. Neurobiol. 43 (2), 133–153. https://doi.org/10.1111/nan.12328.

Ding, Q., et al., 2021. TDP-43 mutation affects stress granule dynamics in differentiated NSC-34 motoneuron-like cells. Front. Cell Dev. Biol. 8 (9), 611601. https://doi.org/10.3389/fcell.2021.611601.

Dragoni, F., et al., 2025. Cross-tissue MiRNA profiling of extracellular vesicles and PBMCs from amyotrophic lateral sclerosis patients. Sci. Rep. 15 (1), 14976. https://doi.org/10.1038/s41598-025-99206-2.

Filareti, M., et al., 2017. Decreased levels of foldase and chaperone proteins are associated with an early-onset amyotrophic lateral sclerosis. Front. Mol. Neurosci. 10, 99. https://doi.org/10.3389/fnmol.2017.00099.

Freischmidt, A., et al., 2015. Serum microRNAs in sporadic amyotrophic lateral sclerosis. Neurobiol. Aging 36 (9). https://doi.org/10.1016/j.neurobiolaging.2015.06.003, 2660.e15-20.

Friedman, R.C., et al., 2009. Most mammalian mRNAs are conserved targets of microRNAs. Genome Res. 19 (1), 92–105. https://doi.org/10.1101/gr.082701.108.

Grima, N., et al., 2023. RNA sequencing of peripheral blood in amyotrophic lateral sclerosis reveals distinct molecular subtypes: considerations for biomarker discovery. Neuropathol. Appl. Neurobiol. 49 (6), e12943. https://doi.org/10.1111/nan.12943.

Gunn, A.P., et al., 2026. Decreased metallothionein-3 expression in the human spinal cord is a common feature of amyotrophic lateral sclerosis and multiple sclerosis. Sci. Rep. 16 (1), 9598. https://doi.org/10.1038/s41598-025-31283-9.

Gwathmey, K.G., et al., 2023. Diagnostic delay in amyotrophic lateral sclerosis. Eur. J. Neurol. 30 (9), 2595–2601. https://doi.org/10.1111/ene.15874.

Hozumi, I., et al., 2008. The expression of metallothioneins is diminished in the spinal cords of patients with sporadic ALS. Amyotroph. Lateral Scler. 9 (5), 294–298. https://doi.org/10.1080/17482960801934312.

Hu, J.H., et al., 2003. Protein kinase and protein phosphatase expression in amyotrophic lateral sclerosis spinal cord. J. Neurochem. 85 (2), 432–442. https://doi.org/10.1046/j.1471-4159.2003.01670.x.

Jakovac, H., et al., 2013. Metallothionein I+II expression as an early sign of chronic relapsing experimental autoimmune encephalomyelitis in rats. Curr. Aging Sci. 6 (1), 37–44. https://doi.org/10.2174/1874609811306010006.

Klim, J.R., et al., 2021. Connecting TDP-43 pathology with neuropathy. Trends Neurosci. 44 (6), 424–440. https://doi.org/10.1016/j.tins.2021.02.008.

Laine, J., et al., 2002. Differential regulation of Akt kinase isoforms by the members of the TCL1 oncogene family. J. Biol. Chem. 277 (5), 3743–3751. https://doi.org/10.1074/jbc.M107069200.

Liguori, M., et al., 2018. Dysregulation of MicroRNAs and target genes networks in peripheral blood of patients with sporadic amyotrophic lateral sclerosis. Front. Mol. Neurosci. 11, 288. https://doi.org/10.3389/fnmol.2018.00288.

Ling, S.C., 2018. Synaptic paths to neurodegeneration: the emerging role of TDP-43 and FUS in synaptic functions. Neural Plast. 2018, 8413496. https://doi.org/10.1155/2018/8413496.

Liu, G., et al., 2017. Endocytosis regulates TDP-43 toxicity and turnover. Nat. Commun. 8 (1), 2092. https://doi.org/10.1038/s41467-017-02017-x.

Livak, K.J., Schmittgen, T.D., 2001. Analysis of relative gene expression data using real-time quantitative PCR and the 2(-Delta Delta C(T)) method. Methods 25 (4), 402–408. https://doi.org/10.1006/meth.2001.1262.

Love, M.I., et al., 2014. Moderated estimation of fold change and dispersion for RNA-seq data with DESeq2. Genome Biol. 15 (12), 550. https://doi.org/10.1186/s13059-014-0550-8.
Luotti, S., et al., 2020. Diagnostic and prognostic values of PBMC proteins in amyotrophic lateral sclerosis. Neurobiol. Dis. 139, 104815. https://doi.org/10.1016/j.nbd.2020.104815.
Mackenzie, I.R., et al., 2007. Pathological TDP-43 distinguishes sporadic amyotrophic lateral sclerosis from amyotrophic lateral sclerosis with SOD1 mutations. Ann. Neurol. 61 (5), 427–434. https://doi.org/10.1002/ana.21147.
Maity, D., Kaundal, R.K., 2025. Exploring dysregulated miRNAs in ALS: implications for disease pathogenesis and early diagnosis. Neurol. Sci. 46 (4), 1661–1686. https://doi.org/10.1007/s10072-024-07840-x.
Marongiu, J., et al., 2026. Corticospinal propagation of full-length TDP-43 toxicity drives brain-to-muscle pathology. bioRxiv. https://doi.org/10.64898/2026.03.27.714692.
Matt, S.M., et al., 2020. Where is dopamine and how do immune cells see it?: dopamine-mediated immune cell function in health and disease. J. NeuroImmune Pharmacol. 15 (1), 114–164. https://doi.org/10.1007/s11481-019-09851-4.
Mead, R.J., et al., 2023. Amyotrophic lateral sclerosis: a neurodegenerative disorder poised for successful therapeutic translation. Nat. Rev. Drug Discov. 22, 185–212. https://doi.org/10.1038/s41573-022-00612-2.
Montalant, A., et al., 2024. Dopamine and noradrenaline activate spinal astrocyte endfeet via D1-like receptors. Eur. J. Neurosci. 59 (6), 1278–1295. https://doi.org/10.1111/ejn.16205.
Mosallaei, M., et al., 2022. PBMCs: a new source of diagnostic and prognostic biomarkers. Arch. Physiol. Biochem. 128 (4), 1081–1087. https://doi.org/10.1080/13813455.2020.1752257.
Nardo, G., et al., 2011. Amyotrophic lateral sclerosis multiprotein biomarkers in peripheral blood mononuclear cells. PLoS One 6 (10), e25545. https://doi.org/10.1371/journal.pone.0025545.
Neumann, M., et al., 2006. Ubiquitinated TDP-43 in frontotemporal lobar degeneration and amyotrophic lateral sclerosis. Science 314 (5796), 130–133. https://doi.org/10.1126/science.1134108.
Paxinos, G., Watson, C., 2006. The Rat Brain in Stereotaxic Coordinates, Hard Cover edition.
Picotti, P., et al., 2007. Amyloid fibril formation and disaggregation of fragment 1-29 of apomyoglobin: insights into the effect of pH on protein fibrillogenesis. J. Mol. Biol. 367 (5), 1237–1245. https://doi.org/10.1016/j.jmb.2007.01.072.
Porta, S., et al., 2018. Patient-derived frontotemporal lobar degeneration brain extracts induce formation and spreading of TDP-43 pathology in vivo. Nat. Commun. 9 (1), 4220. https://doi.org/10.1038/s41467-018-06548-9.
Prasad, A., et al., 2019. Molecular mechanisms of TDP-43 misfolding and pathology in amyotrophic lateral sclerosis. Front. Mol. Neurosci. 12, 25. https://doi.org/10.3389/fnmol.2019.00025.
Puttaparthi, K., et al., 2002. Disease progression in a transgenic model of familial amyotrophic lateral sclerosis is dependent on both neuronal and non-neuronal zinc binding proteins. J. Neurosci. 22 (20), 8790–8796. https://doi.org/10.1523/JNEUROSCI.22-20-08790.2002.
Reale, L.A., et al., 2023. Pathologically mislocalised TDP-43 in upper motor neurons causes a die-forward spread of ALS-like pathogenic changes throughout the mouse corticomotor system. Prog. Neurobiol. 226, 102449. https://doi.org/10.1016/j.pneurobio.2023.102449.
Renton, A.E., et al., 2014. State of play in amyotrophic lateral sclerosis genetics. Nat. Neurosci. 17 (1), 17–23. https://doi.org/10.1038/nn.3584.
Richards, D., et al., 2021. Time to diagnosis and factors affecting diagnostic delay in amyotrophic lateral sclerosis. Amyotroph. Lateral Scler. 2. https://doi.org/10.36255/exonpublications.amyotrophiclateralsclerosis.diagnosticdelay.2021.
Riva, N., et al., 2022. Phosphorylated TDP-43 aggregates in peripheral motor nerves of patients with amyotrophic lateral sclerosis. Brain 145 (1), 276–284. https://doi.org/10.1093/brain/awab285.
Roche, J.C., et al., 2012. A proposed staging system for amyotrophic lateral sclerosis. Brain 135 (Pt 3), 847–852. https://doi.org/10.1093/brain/awr351.
Rossi, D., et al., 2018. CSF neurofilament proteins as diagnostic and prognostic biomarkers for amyotrophic lateral sclerosis. J. Neurol. 265 (3), 510–521. https://doi.org/10.1007/s00415-017-8730-6.
Ru, Y., et al., 2014. The multiMiR R package and database: integration of microRNA-target interactions along with their disease and drug associations. Nucleic Acids Res. 42 (17), e133. https://doi.org/10.1093/nar/gku631.
Shen, S., et al., 2014. rMATS: robust and flexible detection of differential alternative splicing from replicate RNA-Seq data. Proc. Natl. Acad. Sci. USA 111 (51), E5593–E5601. https://doi.org/10.1073/pnas.1419161111.
Staats, K.A., et al., 2022. Blood-based biomarkers of inflammation in amyotrophic lateral sclerosis. Mol. Neurodegener. 17 (1), 11. https://doi.org/10.1186/s13024-022-00515-1.
Staderini, T., et al., 2022. Biophysical characterization of full-length TAR DNA-binding protein (TDP-43) phase separation. Protein Sci. 31 (12), e4509. https://doi.org/10.1002/pro.4509.
Sturmey, E., Malaspina, A., 2022. Blood biomarkers in ALS: challenges, applications and novel frontiers. Acta Neurol. Scand. 146 (4), 375–388. https://doi.org/10.1111/ane.13698.
Vega-Benedetti, A.F., et al., 2024. Immune responses to oligomeric α-synuclein in Parkinson's disease peripheral blood mononuclear cells. J. Neurol. 271 (9), 5916–5929. https://doi.org/10.1007/s00415-024-12554-3 (Epub 2024 Jul 10).
Vivoli Vega, M., et al., 2019. Isolation and characterization of soluble human full-length TDP-43 associated with neurodegeneration. FASEB J. 33 (10), 10780–10793. https://doi.org/10.1096/fj.201900474R.
Wang, X., et al., 2011. A new subtype of progenitor cell in the mouse embryonic neocortex. Nat. Neurosci. 14 (5), 555–561. https://doi.org/10.1038/nn.2807.
Wu, X., et al., 2020. MicroRNA-15a, microRNA-15b and microRNA-16 inhibit the human dopamine D1 receptor expression in four cell lines by targeting 3'UTR −12 bp to + 154 bp. Artif. Cells Nanomed. Biotechnol. 48 (1), 276–287. https://doi.org/10.1080/21691401.2019.1703729.
Yu, S.F., et al., 2025. An ALS assembly modulator signature in peripheral blood mononuclear cells: implications for ALS pathophysiology, therapeutics, and diagnostics. Clin. Proteomics 22 (1), 16. https://doi.org/10.1186/s12014-025-09538-4.
Yuan, D., et al., 2024. Clinical features and progress in diagnosis and treatment of amyotrophic lateral sclerosis. Ann. Med. 56 (1), 2399962. https://doi.org/10.1080/07853890.2024.2399962.

Glossary

ALS: Amyotrophic lateral sclerosis
ALSFRS: ALS Functional Rating Scale–Revised
DEGs: Differentially expressed genes;
PBMCs: Peripheral blood mononuclear cells
TDP-43: TAR DNA-binding protein 43
RT-qPCR: Reverse Transcription Quantitative PCR
PD: Parkinson's Disease
miRNAs: MicroRNAs
AUC: Area under the curve
ROC: Receiver operating characteristic
sALS: Sporadic ALS
fALS: Familial ALS
TARDBP: TAR DNA-binding protein
SOD1: Superoxide dismutase 1
C9orf72: Chromosome 9 open reading frame 72
FUS: Fused in sarcoma
pTDP-43: Phosphorylated TDP-43
CNS: Central nervous system
dsDEGs: Disease-specific DEGs
HCs: Healthy control cases
SEC: Size exclusion chromatography
PCA: Principal component analysis
AS: Alternative splicing
rMATS: Replicate Multivariate Analysis of Transcript Splicing
SD: Standard deviation
CI: Confidence interval
FTLD: Frontotemporal lobar dementia